RSC Advances

ROYAL SOCIETY OF CHEMISTRY

www.rsc.org/advances

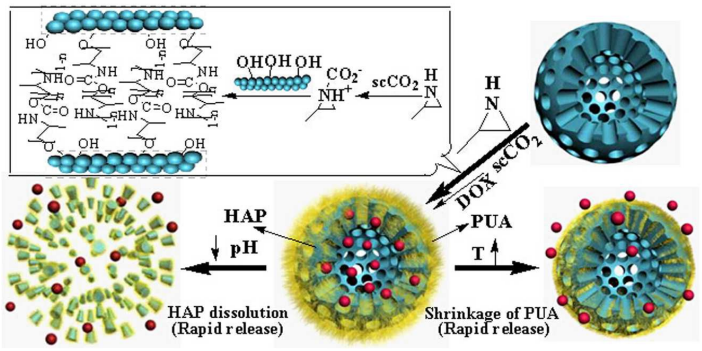

Aliphatic PUA-grafted mesoporous hollow hydroxyapatite microparticles with thermal-responsive on-off gates for controllable drug delivery were prepared via *in situ* polymerization in supercritical CO_2.

Cite this: DOI: 10.1039/coxx00000x

www.rsc.org/xxxxxx

ARTICLE TYPE

In situ functionalization of hollow mesoporous hydroxyapatite with thermal-responsive on-off gates in supercritical CO_2

Qiong Wu, Jun Shi*, Jing Wei, Liu Yang and Shaokui Cao*

Received (in XXX, XXX) Xth XXXXXXXXX 20XX, Accepted Xth XXXXXXXXX 20XX
DOI: 10.1039/b000000x

In this work, aliphatic poly(urethane-amine) (PUA) grafted mesoporous hollow hydroxyapatite (H-HAP) microparticles were prepared via *in situ* polymerization in supercritical CO_2. Thermal-responsive PUA acted as the on-off gates inside the mesoporous H-HAP due to the stretch and shrinkage of the PUA polymer chains at different temperatures. The PUA-grafted hollow HAP (PUA-g-H-HAP) microparticles displayed high specific surface area (95 $m^2 g^{-1}$) and drug loading efficiency (60 %). The *in vitro* drug release studies indicated that PUA-g-H-HAP microparticles exhibited distinguished pH- and thermal-dependent drug release properties, and PUA on-off switches enabled the DOX release in a reversible way by simply adjusting the environmental temperature. Moreover, compared to the hollow HAP microparticles having a higher amount of released DOX over the initial 2 h (about 24.4% of total released drug over 24 h) at 37 ^oC and pH 7.4, PUA-g-H-HAP microparticles displayed a sustained release property with the value of only 10.7% deriving from the blockage of the stretched PUA chains inside the mesoporous H-HAP.

Keywords: Mesoporous HAP; Supercritical CO_2; Aliphatic PUA; Thermal-/pH- responsive; Drug delivery

1. Introduction

During the past decade, mesoporous microparticles have attracted increasing attention because of their unique characteristics such as extraordinarily high specific surface area, large pore volume, tunable pore size and well-defined ordered mesostructure,[1-4] which are crucial for developing new types of drug delivery carriers.[5-9] Anchoring organic molecules on certain inorganic supports has resulted in the design of hybrid carriers that show cooperative functional behaviors.[10,11] More importantly, hollow mesoporous microparticles show more outstanding advantages as drug carriers by incorporating the hollow interior and mesoporous shell into one structure.[12] The hollow interior can provide the space for drug loading and then ensure the high drug loading efficiency. On the other hand, the mesoporous shell can provide the pathway for the drug into/out of the hollow cavity.[13,14]

As a major inorganic constituent of teeth and bones, hydroxyapatite ($Ca_{10}(PO_4)_6(OH)_2$, HAP) has been an excellent candidate for biomedical application because of their outstanding biological activity, biocompatibility and biodegradability.[15,16] The surface modification of mesoporous hollow HAP (H-HAP) microparticles is an efficient way to obtain specific properties and improve the surface activities of HAP.[17] Recently, stimuli-responsive HAP, which obtained via the functionalization of HAP surface with stimuli-responsive polymers, has attracted increasing attention due to their potential applications as the novel functional drug carriers. Li et al. prepared stimuli-responsive hybrid HAP particles by grafting pH-sensitive polystyrene-co-4-vinylpyridine brushes onto HAP.[18] Wei et al. synthesized HAP nanoparticles grafted by thermal-responsive poly(N-isopropylacrylamide) (PNIPAAm) brushes, and the hybrid materials could be used in tissue engineering.[19] As a most widely studied thermal-responsive polymer, PNIPAAm has been extensively employed in biomedicine field.[20,21] However, the poor degradability and potential cytotoxicity should not be ignored, which may bring side effects on the bioactive substances.[22] Aliphatic poly(urethane-amine) (PUA), consisted of hydrophobic urethane and hydrophilic amine unites, shows a thermally induced reversible transition property in aqueous solution at its lower critical solution temperature (LCST) as illustrated in Fig. S1 of the Supporting Information.[23] Compared with PNIPAAm, aliphatic PUA has many potential advantages for the application in biomedicine field. Zdrahala et al. have already performed a series of experiments to vetify the good biodegradabilty, biocompatibility and noncytotoxicity of PUA.[24,25]

Herein, we describe a novel method based on *in situ* functionalization of hollow mesoporous HAP with thermal-responsive aliphatic PUA for smart drug delivery, which shows promising potential as smart drug carrier as shown in Fig. 1. H-HAP microparticles were fabricated by a hydrothermal method using vaterite $CaCO_3$ as a template.[26] $CaCO_3$ core could be easily removed because of the good solubility of $CaCO_3$ in

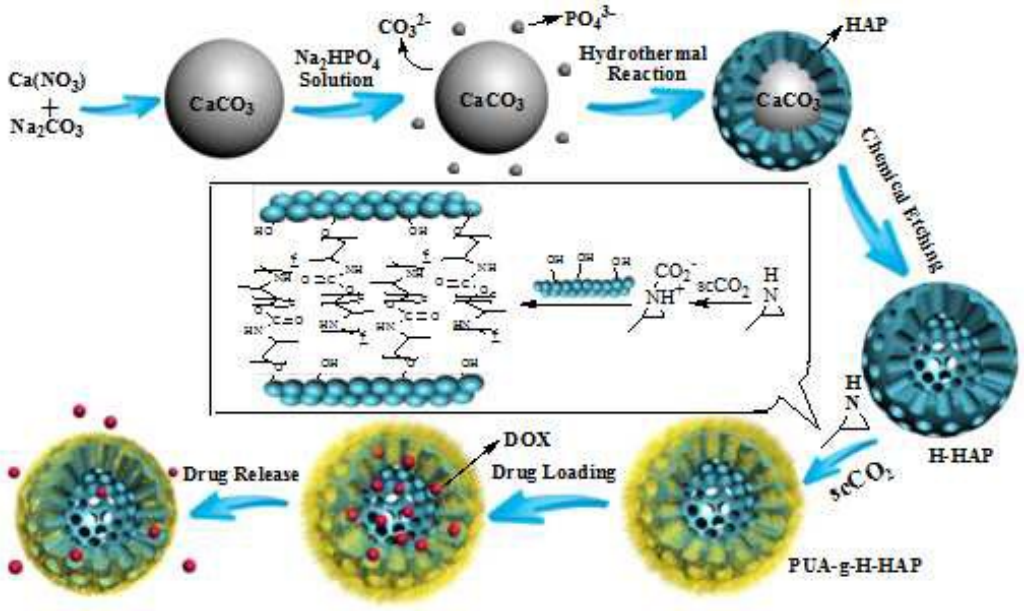

Fig. 1 Preparation of mesoporous PUA-g-H-HAP microparticles with thermal-responsive gates.

acetic acid solution, and the mesoporous H-HAP microparticles were then obtained. Finally, thermal-responsive aliphatic PUA was immobilized within the mesoporous H-HAP microparticles via *in situ* polymerization under supercritical carbon dioxide ($scCO_2$) condition.[27] Compared with conventional polymerization, the above reaction avoided the employment of organic solvents and environmentally friendly CO_2 was used as solvent and reactant in the polymerization process.[28] In addition, the high diffusibility of $scCO_2$ can insure that PUA could be immobilized deeply into the mesoporous H-HAP microparticles. More importantly, aliphatic PUA could form covalent bonds with the HAP matrix for the sake of the interaction between the amino groups of PUA and the hydroxyl groups of HAP, as illustrated in Fig. 1.

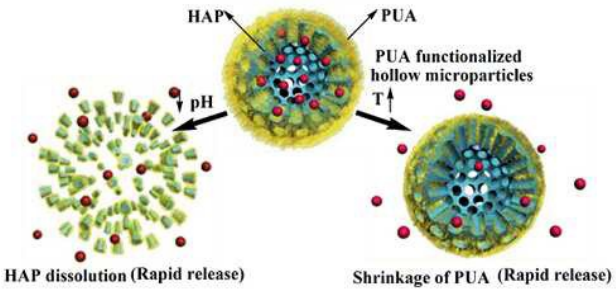

Fig. 2 Schematic illustration of thermal-/pH- responsive drug release from PUA-g-H-HAP microparticles.

In the present design, aliphatic PUA was employed as the thermal-responsive component due to the shrinkage and stretch of the PUA polymer chains at various temperatures, just like a reversible storage gate as well as a release switch as shown in Fig. 2. When the temperature is below LCST, the polymer chains swell and the pores of HAP are closed, resulting in the capture of model drug (doxorubicin hydrochloride, DOX). When the temperature is above LCST, the polymer chains within the pores shrink and the mesoporous shell are exposed, resulting in the rapid release of DOX.[29] Moreover, the drug release of the hollow carriers exhibited distinguished pH-dependent properties due to the dissolution of HAP in the acidic media. More interestingly, compared with the H-HAP microparticles, PUA-grafted hollow HAP (PUA-g-H-HAP) microparticles displayed a distinct sustained release property at 37 °C and pH 7.4 for the sake of the blockage of stretched PUA polymeric chains inside the mesoporous H-HAP microparticles. The present paper provides a facile and green route to fabricate smart hierarchical hybrid hollow drug carriers by combining stimuli-responsive polymers with inorganic mesoporous hollow microparticles, which is highly attractive for controllable drug delivery.

2. Experimental section

2.1. Materials

Sodium poly(styrene sulfonate) (PSS, M_w = 70000, Alfa Organics, China), DL-1-amine-2-propanol (Aladdin Reagent Co. Ltd, China), doxorubicin hydrochloride (DOX, Beijing Huafenglianbo Chemical, China), calcium nitrate ($Ca(NO_3)_2$, Tianjin Chemical Reagent Factory, China), sodium carbonate (Na_2CO_3, Tianjin Hengxing Chemical, China) and disodium hydrogen phosphate dodecahydrate ($Na_2HPO_4 \cdot 12H_2O$, Tianjin Dengke Chemical, China) were analytical reagents and used as received. Commercial CO_2 (99.99% pure) was used without further purification.

2.2. Preparation of H-HAP microparticles

Na_2CO_3 solution (0.1 M, 20 mL) was rapidly poured into $Ca(NO_3)_2$ (0.1 M, 20 mL) and PSS (400 mg) mixed solution under magnetic agitation (1000 rpm). The solution was kept at 30 °C for 30 min. The vaterite $CaCO_3$ microparticles were washed with distilled water for 3 times and then collected by centrifugation. The vaterite $CaCO_3$ was mixed with Na_2HPO_4 solution (0.93 M, 30mL). The suspension was then transferred into 100 mL of autoclave, sealed, and heated by a hydrothermal method at 140 °C for 4 h. When the reaction was finished, the

as-formed HAP having a $CaCO_3$ core was washed with distilled water for 3 times and then collected by centrifugation. By removing the $CaCO_3$ cores with acetic acid (pH 4.5), mesoporous H-HAP microparticles were obtained.

2.3. *In situ* polymerization of aliphatic PUA onto H-HAP microparticles

2-Methylaziridine monomer was synthesized by treating DL-1-amine-2-propanol with sulfuric acid to form the sulfate ester and then cycling the sulfate ester with sodium hydroxide. Then, H-HAP microparticles (50 mg) and 2-methylaziridine (1 mL) were introduced into the autoclave (50 mL) filled with N_2. The reactor was pressurized succeedingly with compressed CO_2 (22 mL) to 10 MPa. After stirring at 100 ^oC for 24 h, the reaction was stopped by cooling the autoclave in an ice bath. The product was washed by methanol for three times and collected by centrifugation. The supernatant was saved and purified by reprecipitation from methanol/ether for the measurement of LCST of aliphatic PUA. The LCST of aliphatic PUA is 50 ^oC as measured by a temperature-variable UV-vis spectrometer. In our previous work, we had synthesized aliphatic PUA by copolymerization of 2-methylaziridine with CO_2 to determine the LCST of pure aliphatic PUA. In the present study, the dissolved aliphatic PUA in reaction medium after *in situ* polymerization reaction was purified to determine the LCST of grafted aliphatic PUA. The results showed that the LCST of PUA from these two different procedures remained the same.

2.4. Characterization of PUA-g-H-HAP microparticles

Transmission electron microscopy (TEM) was carried out on a Tecnai G2 20 emission electron microscope (FEI) using the copper grid as the sample holder operating at 200 kV. The high magnification morphology was observed using field emission scanning electron microscope (FESEM, JSM-7001F). Before FESEM observation, the samples were coated with an approximate 100 Å layer of Gold. FT-IR spectra were recorded with a Nicolet Protégé 460 FT-IR spectrometer in the range of 4000-500 cm^{-1} using KBr pellets. The crystalline phases of samples were examined with X-ray power diffraction (XRD, PHILIPS X'Pert Pro diffractometer) using Cu-Ka radiation (1.54178 Å) with a graphite monochromator. The formation of HAP and the incorporation of PUA and HAP were confirmed by means of scanning electron microscopy (SEM, Philips-quanta-2000) and energy dispersive X-ray spectrometer (EDS). The grafting of PUA onto H-HAP was also measured by X-ray photoelectron spectroscopy (XPS, ESCALAB 250Xi). N_2 adsorption/desorption isotherms were obtained on a Micromeritics ASAP 2020 apparatus. Brunauer-Emmett-Teller (BET) analyses were used to calculate the surface area, pore size, and pore volume. Thermogravimetric analysis (TGA) was carried out on a TGA/DSC 1-Thermogravimetric Analyzer (METTLER TOLEDO) with the heating rate of 10 ^oC min^{-1} under an Ar atmosphere.

2.5. DOX loading and *in vitro* drug release

50 mg of samples was incubated in 4 mL of DOX aqueous solution (0.5 mg mL^{-1}). The suspension was kept at 30 ^oC for 12 h under magnetic agitating. After loading, the samples were rinsed by distilled water for 3 times, collected by centrifugation and then vacuum dried at 40 ^oC for 24 h. The DOX amounts of the clear supernatant were measured by UV-vis absorption spectroscopy at 481 nm and calculated by employing a calibration curve. The encapsulated DOX can be calculated by subtracting the amount of the DOX in the supernatant from the fed DOX amount.

For the *in vitro* drug release test, the DOX-loaded microparticles (10 mg) were suspended in 30 mL of phosphate buffer solution (PBS) with pH 7.4 or HCl solution with pH 2.1 and stirred in a horizontal shaker at 37 or 55 ^oC. The sample (3 mL) were periodically removed for UV-vis analysis and replaced by the same volume of fresh medium. For the further investigation of the reversible thermal-sensitivity, the prepared microparticles were suspended in 30 mL of PBS with pH 7.4. The sample (3 ml) was removed and replaced by the same volume of fresh medium. The temperature was switched between 37 and 55 ^oC every 1.5 h. All the tests were carried out in triplicate and the average values were shown in this study.

3. Results and Discussion

3.1. Characterization of PUA-g-H-HAP hybrid microparticles

In the present work, H-HAP microparticles had been fabricated by a hydrothermal method using PSS-doped vaterite $CaCO_3$ as a template,[30] and the following etching of $CaCO_3$ core. PSS had been used as the crystal growth additive to accelerate the transformation of $CaCO_3$ from calcite to vaterite during the course of $CaCO_3$ preparation.[31] Owing to the presence of abundant hydroxyl groups on the surface of H-HAP, 2-methylaziridine could be impregnated onto the surface of H-HAP microparticles by *in situ* ring-opening polymerization.[27] Therefore, thermal-responsive PUA could covalently anchor onto the surface of mesoporous H-HAP microparticles. The structure and characterization of aliphatic PUA prepared under $scCO_2$ condition has been discussed in detail in other literatures.[23,28]

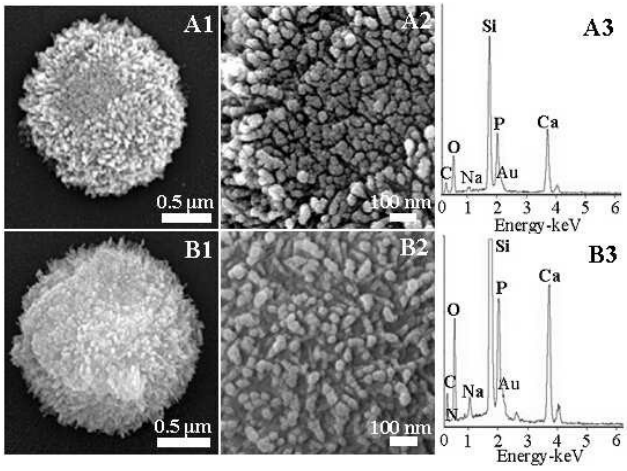

Fig. 3 FESEM micrographs (1, 2) and corresponding EDX spectra (3) of H-HAP microparticles (A) and PUA-g-H-HAP microparticles (B).

Fig. S2 shows the SEM micrographs and corresponding EDX spectra of vaterite $CaCO_3$ and HAP microparticles. The $CaCO_3$ microparticles had been used as the sacrificial templates to fabricate HAP, therefore it was important to control their shape and morphology. With the assistance of PSS, $CaCO_3$

microparticles were uniform spherical with an average diameter of 2 μm (A1). The $CaCO_3$ microparticles could be easily transformed to HAP through ion-exchange method by mixing $CaCO_3$ and Na_2HPO_4 to react at 140 °C for 4 h.[32,33] Compared with $CaCO_3$, the surface of HAP became more coarse and porous than that of $CaCO_3$ ones and the size of HAP was slightly larger because of its looser structure after ion-exchange reaction (B1). The presence of P elements in the EDX spectrum of HAP (B2) indicated the successful formation of HAP.

Fig. 3 shows the FESEM images and corresponding EDX spectra of H-HAP and PUA-g-H-HAP microparticles. After etching with acetic acid, the $CaCO_3$ cores of HAP microparticles were removed and spherical mesoporous H-HAP microparticles with an average diameter of 2 μm (A1) were obtained. Moreover, H-HAP microparticles were consisted of ordered loose mesostructure with pore channels (20 nm of diameter) penetrating from the outside into the inner hollow core according to the higher magnification (A2). After *in situ* polymerization, the structure of the H-HAP microparticles was more compact (B1) and the original channels seemed to be obstructed (B2), indicating the successful incorporation of PUA polymeric chains inside the mesoporous H-HAP microparticles. The corresponding EDX spectrum proved the presence of N element coming from aliphatic PUA.

To further investigate the average particle diameter and diameter dispersity, we selected 30 individual microparticles randomly in the SEM image of the hybrid microparticles and analyzed the diameter dispersity of the microparticles with diameter analysis software. The results showed that the average diameter of the hybrid microparticles was around 1.92 μm and more than half of the microparticles had the diameters ranging from 1.80 and 2.20 μm. The diameter dispersity bar diagram of the hybrid microparticles was shown in Fig. S3.

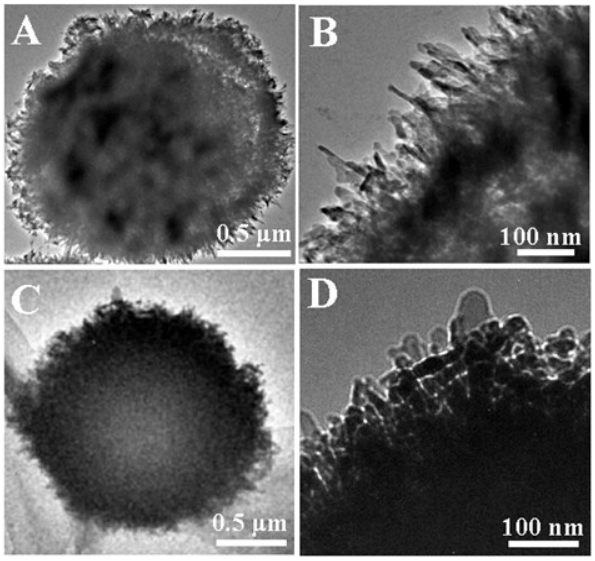

Fig. 4 TEM images of H-HAP (A, B) and PUA-g-H-HAP microparticles (C, D).

Fig. 4 shows TEM micrographs of mesoporous H-HAP (A and B) and PUA-g-H-HAP microparticles (C and D). The surface of H-HAP microparticles was constructed by plenty of HAP nanoneedles with diameter around 10 nm according to the higher magnification TEM image (Fig. 4B). The distinct contrast between the core and the shell could be observed from the PUA-g-H-HAP microparticles (Fig. 4C), indicating the hollow structure of the microparticles. Compared with the TEM image of H-HAP microparticles (Fig. 4A), the outer wall of the PUA-g-H-HAP microparticles was darker for the sake of the incorporation of PUA inside the mesoporous H-HAP microparticles. Moreover, the HAP nanoneedles around the HAP hollow microparticles disappeared and the surface of the hybrid microparticles seemed to be smoother from the higher magnification image (Fig. 4D) because of the successful incorporation of PUA around the surface of H-HAP microparticles.

FIIR spectra also provide clear evidence for the successful grafting of PUA onto H-HAP microparticles. As shown in Fig. 5A, the intense absorption peak at 1033 cm^{-1} was assigned to the stretching vibration PO_4^{3-} groups, and the absorption peaks at 563 and 603 cm^{-1} were ascribed to the bending vibration of $PO4^{3-}$ groups. The characteristic bands of B-type CO_3^{2-} were located at 1457, 1411 and 873 cm^{-1}.[34,35] As compared with H-HAP microparticles, obvious characteristic absorbance peaks of PUA were revealed. The new absorption peek at 2975 cm^{-1} was assigned to the stretching vibration of C-H of methyl group, one peak at 1697 cm^{-1} could be attributed to the stretching vibration of C=O and the band at 1209 cm^{-1} was attributed to the stretching vibration of C-O.[36,37] Thermogravimetric analysis curves of the H-HAP and PUA-g-H-HAP microparticles are shown in Fig. 5B. Both samples showed weight losses below 150 °C that resulted from the physical loss of water. In the range of 150-450 °C, a remarkable weight loss (10.07%) of PUA-g-H-HAP microparticles could be attributed to the polymer decomposition, indicating that the grafted-PUA content in hybrid microparticles was around 10.07% in weight.

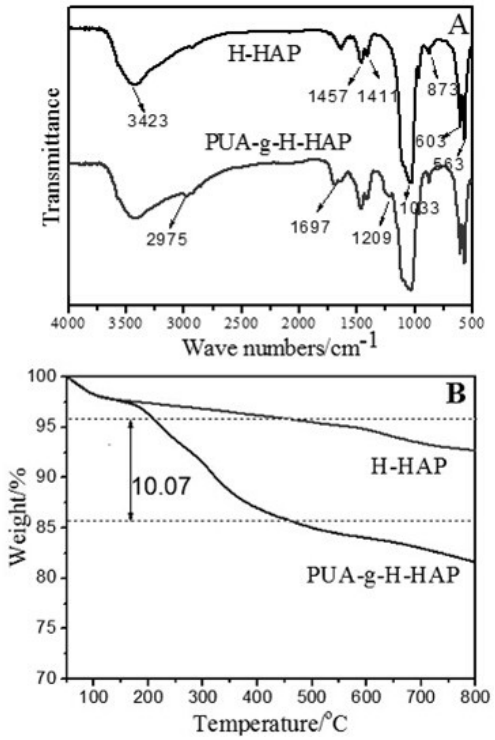

Fig. 5 FT-IR spectra (A) and TGA curves (B) of H-HAP and PUA-g-H-HAP microparticles.

To further demonstrate the successful grafting of PUA onto H-HAP microparticles, the results of X-ray photoelectron spectroscopy (XPS) were also exhibited (Fig. 6). Fig. 6A and B show the survey spectra of ungrafted H-HAP and PUA-grafted H-HAP microparticles. A clear contribution related to the N 1s (400 eV) after grafting reaction could be observed.[38] Fig. 6C and D show the C 1s multiplex scans of H-HAP and PUA-g-H-HAP microparticles, respectively. Both the spectra were decomposed into Gaussian peaks by using a conventional curve-fitting procedure. Three and five peaks were obtained for the ungrafted H-HAP and PUA-g-H-HAP microparticles, respectively. Two new peaks at 287.7 eV and 285.5 eV for the PUA-g-H-HAP microparticles were attributed to C=O and C-N species deriving from aliphatic PUA.[39,40] XPS results further confirmed that PUA had been successfully grafted onto the mesoporous H-HAP microparticles. Fig. S4 presents the XRD patterns of H-HAP and PUA-g-H-HAP microparticles. The characteristic HAP phases could be observed from the resulting samples. It also be noted that $CaCO_3$ phases were also detected because a little amount of $CaCO_3$ were remained after etching process. Moreover, the characteristic diffraction peaks of PUA-g-H-HAP almost remained the same with the XRD curves of H-HAP, which showed that the inorganic part of the hybrid particles retained its original crystal structure after the *in situ* polymerization.

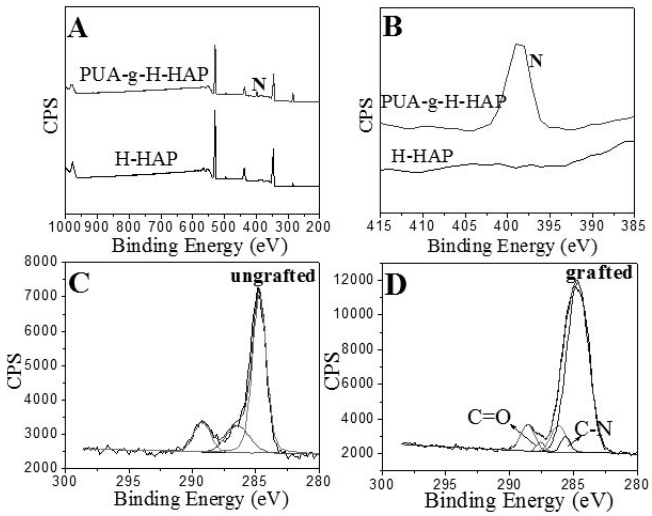

Fig. 6 XPS survey spectra for the ungrafted and PUA-grafted H-HAP microparticles (A and B). XPS C 1s multiplex scans of ungrafted H-HAP (C) and PUA-g-H-HAP (D) microparticles.

N_2 adsorption-desorption isotherms and pore size distribution of H-HAP and PUA-g-H-HAP microparticles are presented in Fig. 7. As shown in Fig. 7A, the isotherms of the two samples could be classified as type IV with a typical H1 hysteresis loop according to the IUPAC classification, indicating the presence of mesoporous structure.[41] The Brunauer-Emmett-Teller (BET) surface area and total pore volume of H-HAP microparticles were calculated to be 115 $m^2\ g^{-1}$ and 0.72 $cm^3\ g^{-1}$, respectively. After grafting PUA onto H-HAP microparticles, the BET surface area and pore volume of PUA-g-H-HAP microparticles were found to be 95 $m^2\ g^{-1}$ and 0.57 $cm^3\ g^{-1}$, respectively. Correspondingly, the Barret-Joner-Halenda (BJH) pore diameters decreased from 24.6 nm to 18.0 nm as shown in Fig. 7B. The noteworthy decrease along with the grafting process could be interpreted as the partial block of microparticle mesopores by PUA polymeric chains.

3.2. DOX loading and sustained release

PUA-g-H-HAP microparticles have the potential to be employed as the excellent drug vehicles with high drug loading efficiency and controllable release properties. Therefore, we further investigate the controlled release property of the PUA-g-H-HAP microparticles. DOX is selected as a model drug to evaluate the loading and release capabilities of the prepared hybrid microparticles because its properties are well documented and it is widely used as an anti-cancer drug. The drug loading efficiency of PUA-g-H-HAP microparticles was about 60% and the drug content was about 0.26 mg per 10 mg sample. It was clear that the inner hollow space played an important role in improving the specific surface area and then enhancing the drug loading efficiency of hybrids.[42] Compared with that of pure HAP microparticles, the drug content of the prepared hybrid microparticles (60%) was relatively low. The possible reason is that the grafted PUA chains would hinder the DOX diffusion during the drug loading process. However, it must be noted that the loaded DOX would be difficult to diffuse into outer release medium from the hybrid microparticles because of the introduction of PUA. In other words, the hybrid microparticles would possess better sustained release property than that of pure HAP microparticles, which will be discussed in the following section.

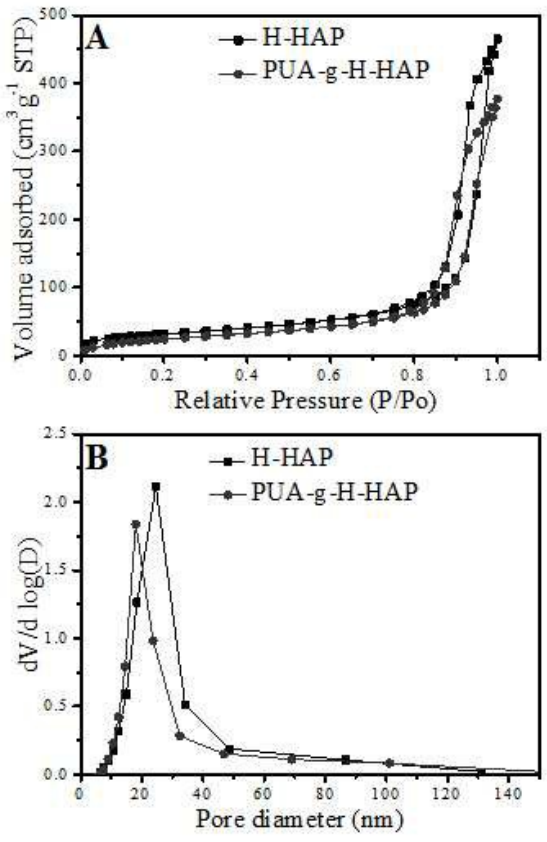

Fig. 7 N_2 adsorption/desorption isotherms of H-HAP and PUA-g-H-HAP microparticles (A) and the corresponding pore size distribution curves (B).

Fig. 8A shows the DOX release amount curves of H-HAP and PUA-g-H-HAP microparticles 37 °C and pH 7.4. The DOX release amount of PUA-g-H-HAP microparticles exhibited a slow and constant tendency. However, the curve of H-HAP microparticles exhibited the distinct initial burst release. The amount of DOX released from PUA-g-H-HAP microparticles over the initial 1 h was about 6.5%, while the value was 13.9% for H-HAP microparticles under the same condition. H-HAP microparticles showed a rapidly released behavior and the cumulative release amount of DOX was 55.2% within 24 h at 37 °C and pH 7.4, while for PUA-g-H-HAP microparticles, the value was only 24.8% at the same condition. The results demonstrated that PUA-g-H-HAP microparticles displayed a distinct sustained release property at 37 °C and pH 7.4 because the stretched PUA polymeric chains would block the mesopores inside the H-HAP microparticles. The *p* value obtained from Student's t-test analysis for the two curves in Fig. 8A was less than 0.0001. The *in vitro* drug release investigation demonstrated that the grafted-PUA inside the hybrid mesoporous microparticles could reduce the drug release rate and assuage the initial burst release of DOX from H-HAP matrix.[29]

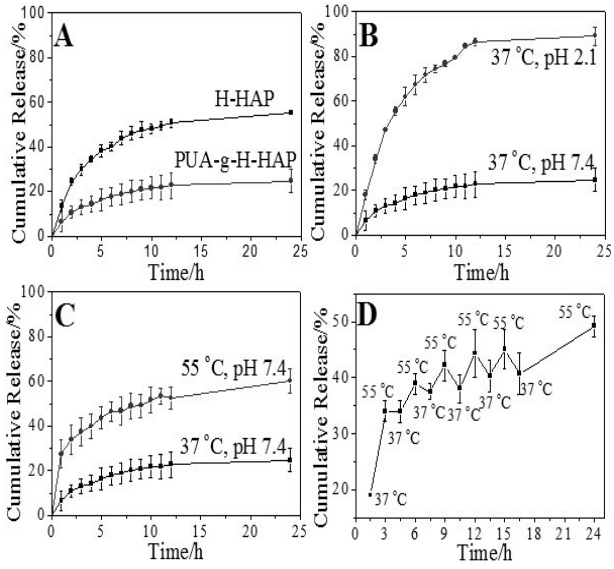

Fig. 8 DOX release profiles of H-HAP and PUA-g-H-HAP microparticles (A), pH-responsive drug release of PUA-g-H-HAP microparticles at 37°C (B), thermal- dependent release profiles of PUA-g-H-HAP microparticles at pH 7.4 (C) and thermal-reversible dependent release profiles of PUA-g-H-HAP microparticles at pH 7.4 (D).

3.3. pH-/Thermal-responsive drug release

Fig. 8B shows the pH-dependent release properties of PUA-g-H-HAP hybrid microparticles at 37 °C. In the present study, phosphate buffer solution (PBS) with pH 7.4 was selected as the drug release medium because the pH value of the normal physiological environment in human body was pH 7.4. HCl solution with pH 2.1 was employed as the contrast pH condition to demonstrate the pH responsiveness of the prepared hybrid microparticles. It could be observed that the DOX release increased with decreasing pH value from 7.4 to 2.1. Only 24.8 % of DOX were released at pH 7.4 over 24 h, but almost 89.2% of DOX were released at pH 2.1 with the same treatment. As illustrated in Fig. 2, the rapid release PUA-g-H-HAP microparticles at pH 2.1 was partly due to the dissolution of HAP in the strong acidic solution.[37] The *p* value obtained from Student's t-test analysis in the comparison between the release at pH 7.4 and 2.1 was less than 0.0001.

The *in vitro* release curves of PUA-g-H-HAP microparticles in response to temperature changes are shown in Fig. 8C. The LCST of aliphatic PUA employed in the present study was around 50 °C. Therefore, we chose 37 and 55 °C as the temperature conditions in drug release study.[30] At 37 °C, the drug release reached at 6.47% over the initial 1h due to the blocking effect of the loose polymer chains in the mesopores of H-HAP microparticles. In contrast, about 27.40% loaded drug was released within 1h at 55 °C because of the rapid shrinkage of polymer chains. Moreover, the drug release was 60.18% at 55 °C over 24 h, which was 40% higher than that at 37 °C. As illustrated in Fig. 9, the PUA chains are swollen when the temperature is below the LCST of PUA. The mesoporous H-HAP microparticles are covered by the stretched PUA polymeric chains, resulting in the slow drug release. In contrast, at temperature above the LCST (55 °C), the grafted-PUA chains are shrunken and the mesopores of H-HAP microparticles are opened because of the shrinking of PUA, which results in the fast drug release.[20,29] The above results verified that the grafted-PUA chains inside the mesoporous H-HAP microparticles act successfully as the thermal-sensitive gates for DOX release. This thermal-dependent "on/off" characteristics enables the drug release in a controlled way by simply adjusting the environmental temperature. The *p* value between the release at 55 and 37 °C was less than 0.0001.

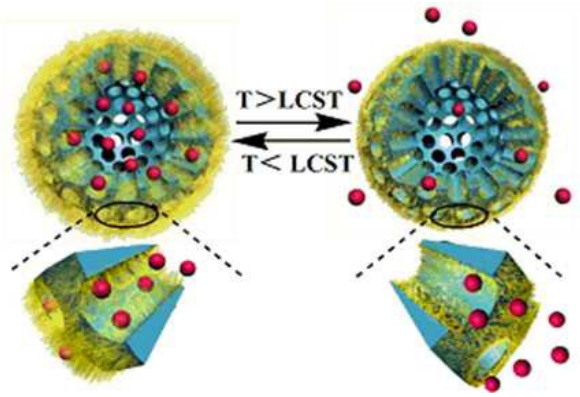

Fig. 9 Thermal-reversible release mechanism of PUA-g-H-HAP microparticles.

3.4. Reversibility of drug release

The main reason for explaining the higher release rate for PUA-g-H-HAP hybrid microparticles at 55 °C was the precipitation of PUA above its LCST, which leaded to the gating effect of the drug delivery. Instead of precipitating from the microparticle bulk as discussed in other inorganic/polymeric hybrid drug carries,[36,37] the shrinkage of PUA in the present design would not break the intact structure of H-HAP microparticles because PUA chains were mostly attached on the surface of mesoporous H-HAP. Therefore, it could be speculated that the better thermal-reversibility could be obtained from PUA-g-H-HAP hybrid microparticles for the sake of its excellent thermal-gating effect. To demonstrate this opinion, the reversible

drug release through the PUA-grafted H-HAP microparticles in response to temperature changes was measured at pH 7.4 with temperature alternating between 37 and 55 ^{o}C.[38] In the experiment, PUA-g-H-HAP microparticles were treated for the first 1.5 h at 37 ^{o}C. Then the samples were moved to another shaker with 55 ^{o}C. This drug release experiment with temperature alternating between 37 and 55 ^{o}C was performed for 22.5 h, and then a thermal-responsive release profile was obtained as described in Fig. 8D. It could be found a clear zigzag-like release pattern could be observed and the drug release was relatively low when the samples were placed in 37 ^{o}C, and the value significantly increased when the samples were placed in 55 ^{o}C. The above results demonstrated that the distinguished reversible thermal-dependent "on/off" characteristics could be obtained from PUA-g-H-HAP hybrid microparticles for the sake of its excellent thermal-gating effect and the studied hybrid microparticles have the potential to be used as a novel "smart" vehicle for controlled drug delivery.

The pH-/thermal-responsive drug release results demonstrate that the obtained drug carrier has the potential to be employed as the smart parenteral formulation because these hybrid microparticles could completely meet the dimensional requirement of parenteral formulation. In addition, pH-/thermal-responsive properties achieved via the adjustment of environmental pH values and temperatures are also feasible for the parenteral application.

3.5. Drug release kinetics

The kinetics of DOX release from the hybrid PUA-g-H-HAP microparticles has been analyzed by plotting the cumulative release data versus time by plotting them to the following empirical equation:

$$M_t/M_\infty = kt^n \quad (1)$$

here, M_t is the cumulative amounts of DOX released at time t, and M_∞ is the total released amount of DOX, k is a constant characteristic relating to the microparticles, and n is the diffusion exponent characterizing the nature of the release mechanism.[42,43] The DOX release kinetics of the hybrid PUA-g-H-HAP microparticles at different conditions was analyzed and the values of n, k, and correlation coefficient (R^2) were shown in Table S1. The four formulations exhibited n values ranging from 0.240 to 0.481, indicating the Fickian diffusion was the dominated diffusion mechanism.

In order to accurately understand the kinetics of drug release of the carriers, the n values were further determined from the slope of the $\ln(M_t/M_\infty)$ plot versus ln t. Fig. S5A shows the curves of $\ln(M_t/M_\infty)$ versus ln t for H-HAP and PUA-g-H-HAP microparticles at 37 ^{o}C and pH 7.4. The n values of H-HAP microparticles ranged from 0.852 to 0.408 and produced a shift from Case-II transport to Fickian diffusion. At the same condition, the PUA-g-H-HAP microparticles had the n values ranging from 0.771 to 0.412, indicating a shift from anomalous transport to Fickian diffusion. This may be due to the grafting of PUA chains onto H-HAP microparticles. Fig. S5B shows the curves of $\ln(M_t/M_\infty)$ versus ln t for PUA-g-H-HAP microparticles at different pH values and temperatures. When the temperature was at 37 ^{o}C and pH 2.1, the n value for the hybrid microparticles ranged from 0.806 to 0.436, and the invariant anomalous transport was probably contributed to the quick dissolution of HAP in acetic acid solution. The n values for the hybrid microparticles at 55 ^{o}C and pH 7.4 ranged from 0.898 to 0.263, indicating a shift from Case-II transport to Fickian diffusion, which may be due to the rapid shrinkage of polymer chains. The results indicated that the introduction of PUA had changed the release kinetics of DOX and obstructed the diffusion of loaded drug into the solution.

4. Conclusions

In conclusion, we have developed a novel dual-responsive controlled drug carrier by grafting thermal-responsive polymer aliphatic PUA onto the channel and outer surface of hollow HAP microparticles via *in situ* polymerization under supercritical CO_2 condition. The prepared PUA-g-H-HAP microparticles were composed of a hollow mesoporous HAP shell and thermal-responsive PUA polymeric gates. The drug release results showed that the PUA-g-H-HAP microparticles exhibited sustained and pH/thermal-responsive drug release property, and PUA on-off gates enabled the DOX release in a reversible way by simply adjusting the environmental temperature. The results demonstrate that the developed hybrid PUA-g-H-HAP microparticles show the great potential as a novel drug carrier for controllable drug delivery.

Acknowledgements: This work was financially supported by the National Natural Science Foundation of China (Projects 20874090 and 21074119) .

Notes and References

† *School of Materials Science and Engineering, Zhengzhou University, Zhengzhou 450052, China*

* *Correspondence author: Jun Shi or Shaokui Cao (E-mail: shijun@zzu.edu.cn, caoshaokui@zzu.edu.cn)*

†Electronic Supplementary Information (ESI) available: Preparation of pH-/thermal- dual responsive aliphatic PUA (Fig. S1). SEM and EDS results of $CaCO_3$ and HAP microparticles (Fig. S2). SEM image of PUA-g-H-HAP microparticles and corresponding diameter dispersity bar diagram (Fig. S3). XRD curves of H-HAP and PUA-g-H-HAP microparticles (Fig. S4). Plots of ln (M_t/M_∞) versus ln t for the release profiles of H-HAP and thermal-responsive PUA-g-H-HAP microparticles at different pH values and temperatures (Fig. S5). Parameters n and R^2 determined by Eq. (1) for the DOX release of samples at different release conditions (Table S1).

1 M. Hartmann, *Chem. Mater.*, 2012, **17**, 4577-4593.
2 A. Stein, *Adv. Mater.*, 2003, **15**, 763-775.
3 I. I. Slowing, B. G. Trewyn, S. Giri and V. S. Y. Lin, *Adv. Funct. Mater.*, 2007, **17**, 1225-1236.
4 M. Vallet-Regí, F. Balas and D. Arcos, *Angew. Chem. Int. Ed.*, 2007, **46**, 7548-7558.
5 C. Argyo, V. Weiss, C. Bräuchle and T. Bein, *Chem. Mater.*, 2014, **26**, 435-451.
6 P. Kovakčík, M. Singh and F. Štěpánek, *Chem. Eng. J.*, 2013, **232**, 591-598.
7 I. I. Slowing, J. L. Vivero-Escoto, C. W. Wu and V. S. Y. Lin, *Adv. Drug. Deliv. Rev.*, 2008, **60**, 1278-1288.
8 R. J. Mudakavi, A. M. Raichur and D. Chakravortty, *RSC Adv.*, 2014, **4,** 61160-61166.
9 D. Arcoc, A. López-Noriega, E. Ruiz-Hernández, O. Terasaki and M. Vallet-Regí, *Chem. Mater.*, 2009, **21**, 1000-1009.

10 A. Rammohan, L. Tayal, A. Kumar, S. Sivakumar and A. Sharma, *RSC Adv.*, 2013, **3**, 2008-2016.
11 Z. Y. Zhou, S. M. Zhu and D. Zhang, *J. Mater. Chem.*, 2007, **17**, 2428-2433.
12 Y. S. Li and J. L. Shi, *Adv. Mater.*, 2014, **26**, 3176-3205.
13 Y. F. Zhu, J. L. Shi, W. H. Shen, X. P. Dong, J. W. Feng, M. L. Ruan and Y. S. Li, *Angew. Chem. Int. Ed.*, 2005, **44**, 5083-5087.
14 G. X. Yang, S. L. Gai, F. Y. Qu and P. P. Yang, *ACS Appl. Mater. Interfaces*, 2013, **5**, 5788-5796.
15 Y. P. Guo, Y. Zhou, D. C. Jia and H. X. Tang, *Microporous and Mesoporous Mater.*, 2009, **118**, 480-488.
16 D. D. Li, Y. T. Zhu and Z. Q. Liang, *Mater. Res. Bull.*, 2013, **48**, 2201-2204.
17 J. C. Wei, A. Liu, L. Chen, P. B. Zhang, X. S. Chen and X. B. Jing, *Macromol. Biosci.*, 2009, **9**, 631-638.
18 C. F. Li, X. L. Ge, S. G. Liu, G. C. Li, A. J. Zhang, J. H. Bai, C. H. Su and R. Ding, *Powder Technol.*, 2011, **210**, 167-174.
19 J. C. Wei, P. He, A. X. Liu, X. S. Chen, X. H. Wang and X. B. Jing, *Macromol. Biosci.*, 2009, **9**, 1237-1246.
20 J. P. Yang, D. K. Shen, L. Zhou, W. Li, X. M. Li, C. Yao, R. Wang, A. M. El-Toni, F. Zhang and D. Y. Zhao, *Chem. Mater.*, 2013, **25**, 3030-3037.
21 C. W. Pester, A. Konradi, B. Varnholt, P. V. Rijn and A. Böker, *Adv. Funct. Mater.*, 2012, **22**, 1724-1731.
22 H. Vihola, A. Laukkanen, L. Valtola, H. Tenhu and J. Hirvonen, *Biomaterials*, 2005, **26**, 3055-3064.
23 O. Ihata, Y. Kayaki and T. Ikariya, *Angew. Chem. Int. Ed.*, 2004, **43**, 717-719.
24 R. J. Zdrahala and I. J. J. Zdrahala, *Biomater. Appl.*, 1999, **14**, 67-90.
25 E. M. Rosenbauer, M. Wagner, A. Musyanovych and K. Landfester, *Macromolecules*, 2010, **43**, 5083-5093.
26 Y. J. Guo, Y. Y. Wang, T. Chen, Y. T. Wei. L. F. Chu and Y. P. Guo, *Mater. Sci. Eng., C*, 2013, **33**, 3166-3172.
27 P. López-Aranguren, L. F. Vega and C. Domingo, *Chem. Commun.*, 2013, **49**, 11776-11778.
28 O. Ihata and Y. Kayaki, *Macromolecules*, 2005, **38**, 6429-6434.
29 X. Zhang, P. P. Yang, Y. L. Dai, P. A. Ma, X. J. Li, Y. Y. Cheng, Z. Y. Hou, X. J. Kang, C. X. Li and J. Lin, *Adv. Funct. Mater.*, 2013, **23**, 4046-4078.
30 Y. J. Guo, Y. Y. Wang, T. Chen, Y. T. Wei, L. F. Chu, Y. P. Guo, *Mater. Sci. Eng., C*, 2013, **33**, 3166-3172.
31 Y. S. Wang, Y. X. Moo, C. P. Chen, P. Gunawan and R. Xu, *J. Colloid Interface Sci.*, 2010, **352**, 393-400.
32 J. Zhang, A. Kumbhar, J. B. He, N. C. Das, K. K. Yang, J. Q. Wang, H. Wang, K. L. Stokes and J. Y. Fang, *J. Am. Chem. Soc.*, 2008, **130**, 15203-15209.
33 P. H. C. Camargo, Y. H. Lee, U. Jeong, Z. Q. Zou and Y. N. Xia, *Langmuir*, 2007, **23**, 2985-2992.
34 Y. P. Guo, T. S. Lin, Y. Zhou, D. C. Jia and Y. J. Guo, *Microporous and Mesoporous Mater.*, 2010, **127**, 245-249.
35 R. N. Panda, M. F. Hsieh, R. J. Chung and T. S. Chin, *J. Phys. Chem. Sol.*, 2003, **64**, 193-199.
36 C. Du, J. Shi, J. Shi, L. Zhang and S. K. Cao, *Mater. Sci. Eng., C*, 2012, **33**, 3745–3752.
37 S. H. Xu, J. Shi, D. S. Feng, L. Yang and S. K. Cao, *J. Mater. Chem., B*, 2014, **2**, 6500-6507.
38 J. Shi, X. P. Liu, X. M. Sun and S. K. Cao, *Polym. Adv. Technol.*, 2011, **22**, 1539-1546.
39 M. L. Chen, M. D. Dong, R. Havelund, V. R. Regina, R. L. Meyer, F. Besenbacher and P. Kingshott, *Chem. Mater.*, 2010, **22**, 4214-4221.
40 J. Shi, N. M. Alves and J. F. Mano, *Adv. Funct. Mater.*, 2007, **17**, 3312-3318.
41 B. S. Tian and C. Yang, *J. Nanosci. Nanotechnol.*, 2011, **11**, 1871-1879.
42 D. S. Feng, J. Shi, X. J. Wang, L. Zhang and S. K. Cao, *RSC Adv.*, 2013, **3**, 24975-24982.
43 P. L. Ritger and N. A. Peppas, *J. Controlled Release*, 1987, **5**, 37-42.